

# **IEICE** **TRANSACTIONS**

## **on Communications**

**VOL. E97-B NO.  
OCTOBER 2014**

**The usage of this PDF file must comply with the IEICE Provisions on Copyright.**

**The author(s) can distribute this PDF file for research and educational (nonprofit) purposes only.**

**Distribution by anyone other than the author(s) is prohibited.**

**A PUBLICATION OF THE COMMUNICATIONS SOCIETY**



The Institute of Electronics, Information and Communication Engineers  
Kikai-Shinko-Kaikan Bldg., 5-8, Shibakoen 3chome, Minato-ku, TOKYO, 105-0011 JAPAN

## PAPER

# Specific Absorption Rates and Temperature Elevations due to Wireless Radio Terminals in Proximity to a Fetus at Gestational Ages of 13, 18, and 26 Weeks

Akihiro TATENO<sup>†a)</sup>, *Student Member*, Shimpei AKIMOTO<sup>††</sup>, Tomoaki NAGAOKA<sup>†††</sup>, Kazuyuki SAITO<sup>††††</sup>, Soichi WATANABE<sup>†††</sup>, *Members*, Masaharu TAKAHASHI<sup>††††</sup>, *Senior Member*, and Koichi ITO<sup>††††</sup>, *Fellow*

**SUMMARY** As the electromagnetic (EM) environment is becoming increasingly diverse, it is essential to estimate specific absorption rates (SARs) and temperature elevations of pregnant females and their fetuses under various exposure situations. This study presents calculated SARs and temperature elevations in a fetus exposed to EM waves. The calculations involved numerical models for the anatomical structures of a pregnant Japanese woman at gestational stages of 13, 18, and 26 weeks; the EM source was a wireless portable terminal placed close to the abdomen of the pregnant female model. The results indicate that fetal SARs and temperature elevations are closely related to the position of the fetus relative to the EM source. We also found that, although the fetal SAR caused by a half-wavelength dipole antenna is sometimes comparable to or slightly more than the International Commission Non-Ionizing Radiation Protection guidelines, it is lower than the guideline level in more realistic situations, such as when a planar inverted-F antenna is used. Furthermore, temperature elevations were significantly below the threshold set to prevent the child from being born with developmental disabilities.

**key words:** fetus, specific absorption rate (SAR), temperature elevation, wireless radio terminals, finite-difference time-domain (FDTD) method

## 1. Introduction

Recently, there has been rapid expansion in the use of portable telecommunications technology based on electromagnetic (EM) waves. Consequently, there has been growing interest in evaluating interactions between EM fields (EMFs) and the human body. When EM energy with frequencies above 100 kHz is absorbed by the body, the primary effect is thermal heating. The specific absorption rate (SAR) continues to be used as the standard dosimetric parameter for setting international safety guidelines for human exposure to RF energy [1], [2]. However, because of the difficulties in obtaining actual measurements, value of SAR in a human body is usually estimated by numerical simulations. Nowadays, anatomically correct computational hu-

man models [3]–[5] allow us to numerically estimate human body SARs with high accuracy.

Recently, the effects of EM waves radiated from antennas held by pregnant females have become a major concern for EM safety, especially as these waves can impact the fetus [6]. Togashi et al. [7] have calculated SARs for a fetus exposed to a half-wavelength dipole antenna and a planar inverted-F antenna (PIFA) with a metallic case at 900 MHz and 2 GHz; these are typical frequency bands of third generation communication systems. In their study, they used a model of a 26th-gestational week pregnant female. Akimoto et al. [8] have calculated the local SAR and temperature elevation for a fetus when a normal-mode helical antenna on a metallic box was placed at the sides of the abdomen of a female who was in the 26th gestational week of pregnancy. Body types and anatomical structures of the mother and fetus differ depending on the stage of fetal growth. Therefore, evaluations for various gestation ages are important, but they have not been reported for near-field exposure, although Nagaoka et al. [9], Dimbylow [10], and Dimbylow et al. [11] have reported results for far-field exposure.

In this study, we present calculated SARs and temperature elevations for fetuses of pregnant female models [12] in the 13th, 18th, and 26th gestational week. The sources of EM radiation were a half-wavelength dipole antenna and a PIFA with a metallic case. Based on guideline set by the International Commission for Non-ionizing Radiation Protection (ICNIRP), the values of the averaged SAR and peak 10-g-averaged SAR for general public exposure should be less than 0.08 W/kg and 2 W/kg, respectively [1]. However, the guidelines do not set any limiting values for fetuses. Therefore, we evaluated fetal temperature elevations caused by the absorption of EM radiation; temperature elevations serve as the basis for setting SAR guidelines and the index of the threshold for thermal effects on fetuses.

## 2. Calculation Method

### 2.1 Numerical Model of a Pregnant Female

Figure 1 illustrates the pregnant female models and the fetuses in the 13th, 18th, and 26th gestational weeks [12]. Table 1 lists the biological dielectric properties of intrinsic parts of the pregnant female model. The body weight

Manuscript received December 16, 2013.

Manuscript revised May 28, 2014.

<sup>†</sup>The author is with the Graduate School of Engineering, Chiba University, Chiba-shi, 263-8522 Japan.

<sup>††</sup>The author is with the Information Technology R&D Center, Mitsubishi Electric Corporation, Kamakura-shi, 247-8501 Japan.

<sup>†††</sup>The authors are with the Applied Electromagnetic Research Institute, National Institute of Information and Communications Technology, Koganei-shi, 184-8795 Japan.

<sup>††††</sup>The authors are with the Center for Frontier Medical Engineering, Chiba University, Chiba-shi, 263-8522 Japan.

a) E-mail: a.tateno@chiba-u.jp

DOI: 10.1587/transcom.E97.B.2175

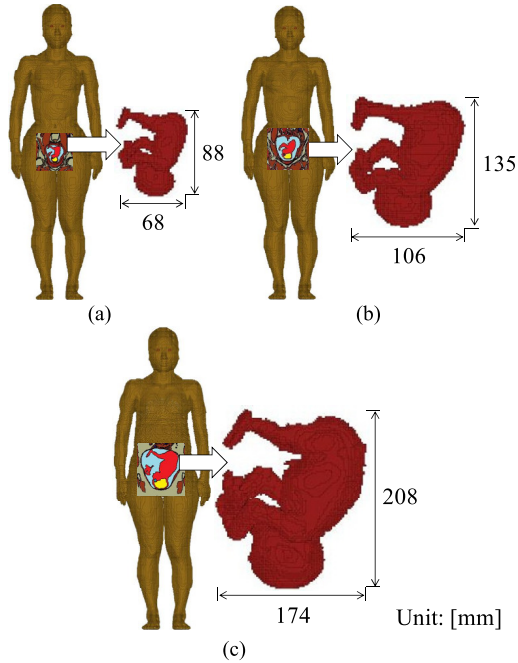


**Fig. 1** Illustrate of numerical models of a (a) 13th, (b) 18th, and (c) 26th gestational week pregnant Japanese female.

**Table 1** Biological dielectric properties of intrinsic parts of a pregnant female.

Tissues and organs	900 MHz		2 GHz	
	Relative Permittivity $\epsilon_r$	Conductivity $\sigma$ [S/m]	Relative Permittivity $\epsilon_r$	Conductivity $\sigma$ [S/m]
Fetal body	62.9	1.17	60.4	1.89
Fetal brain	60.9	1.16	59.4	1.67
Fetal eyes	68.9	1.64	68.5	2.16
Amniotic fluid	71.6	1.60	70.9	2.19
Placenta	59.6	1.26	58.3	1.85

**Table 2** Densities of fetal tissues. [kg/m<sup>3</sup>]

Tissues of fetus	13th gestational week model	18th gestational week model	26th gestational week model
Body	970	970	980
Eyes	970	970	980
Brain	1,018	1,024	1,028

of the fetus and the scale of the maternal abdomen in each model correspond to the standard body weight and scale at each gestational age, respectively. The relative permittivity and conductivity of the fetal body were defined on the basis of values obtained for a rabbit [13]. Values for the fetal brain were adjusted to account for the higher water content in adult brains [14]. A value for the fetal eyes was based on that for the eyes of an adult reported by [15]. Values for the amniotic fluid and placenta were taken from [16]. Values for the other 51 organs were taken from [15], while densities of fetal tissues were taken from [12]. As listed in Table 2, different densities were used for the fetal body, eyes, and brain in each of the three models to match the body weights of the fetuses to reference values [17]. The remaining densities were taken from [18].

**Table 3** Thermal properties of intrinsic parts of a pregnant female.

Tissues and organs	Specific heat $c$ [J/kg·K]	Thermal conductivity $\kappa$ [W/m·K]	Metabolic heat generation $A$ [W/m <sup>3</sup> ]	Term associated with blood flow $B$ [W/m <sup>3</sup> ·K]
Fetal body	3,105	0.39	461	2,729
Fetal brain	3,672	0.53	7,100	39,116
Fetal eyes	4,178	0.59	-	-
Amniotic fluid	3,840	0.50	-	-
Placenta	3,840	0.50	22,900	114,216

## 2.2 Calculation Method

In the numerical calculations, we used the finite-difference time-domain (FDTD) method, which is a commonly-used and efficient method for evaluating the amount of EM wave exposure. To calculate SAR, we used the following equation:

$$\text{SAR} = \frac{\sigma}{\rho} E^2 \quad (1)$$

where  $\sigma$  is the tissue conductivity (S/m),  $\rho$  is the tissue density (kg/m<sup>3</sup>), and  $E$  is the internal electric field strength (V/m). SAR is related to the heating created by the electric field in the tissue, which causes the temperature in the tissue to increase. The temperature elevation in the fetus is then calculated. To determine this temperature elevation, we used a bioheat transfer equation [19],

$$\rho c \frac{\partial T}{\partial t} = \kappa \nabla^2 T + A - B(T - T_b) + \rho \cdot \text{SAR} \quad (2)$$

where  $T$  is the temperature (K),  $t$  is time (s),  $\rho$  is the density (kg/m<sup>3</sup>),  $c$  is the specific heat of the tissue (J/kg·K),  $\kappa$  is the thermal conductivity of the tissue (W/m·K),  $A$  is the metabolic heat generation (W/m<sup>3</sup>),  $B$  is a term associated with blood flow (W/m<sup>3</sup>·K), and  $T_b$  is the blood temperature (K). Values for these parameters of intrinsic tissues in a pregnant female are listed in Table 3 [15], [18], [20]–[27]. Values for the other parameters were taken from [18], [26] and [27]. In the simulations, EM waves from the antenna were continually radiated until the temperature elevation reached a steady state. As the boundary condition of air and the human body, we used Newton's law of cooling as the following.

$$-\kappa \frac{\partial T}{\partial n} = h(T_s - T_a) \quad (3)$$

where  $h$  is the heat transfer coefficient (W/m<sup>2</sup>·K),  $T_s$  is the surface temperature of the tissue (K),  $T_a$  is the temperature of the air (K), and  $n$  is the normal unit vector of the surface on the human body. A detailed explanation of this simulation is given in [28].

Assuming that the EM radiator was a mobile phone, we first used a half-wavelength dipole antenna as the simplest EM radiator. Then, to evaluate the model under more practical conditions, we used a PIFA with a metallic case. Endo et al. [29] compared results from SAR calculations using the FDTD method with measured values obtained when

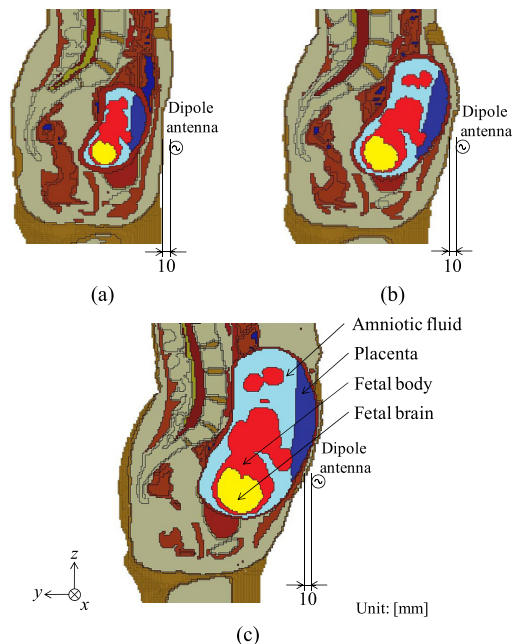


**Fig. 2** Positions of dipole antennas in the sagittal plane including the feeding gap. Model at (a) 13th, (b) 18th, and (c) 26th gestational weeks.

a PIFA with a metallic case was placed in the vicinity of a tissue-equivalent phantom. Endo et al. [29] observed good the agreement between the measured and calculation results. We confirmed that our SAR calculations correspond to the results of Endo et al. [29] under the same conditions.

Togashi et al. [7] estimated the fetal SARs when a dipole antenna was placed at various points around the abdomen of a pregnant female model. Those results showed that the fetal SARs are the highest when the dipole antenna was placed in front of the abdomen. Therefore, the half-wavelength dipole antenna was placed in front of the abdomen of the pregnant female model for the worst-case study of the fetus, as shown in Fig. 2. Furthermore, in [7], the dipole antenna was placed vertically and the distance between the dipole antenna and the model surface was 40 mm, because otherwise, the top of the antenna would penetrate the abdomen. However, that distance was too large for us to evaluate the worst-case scenario. Therefore, to avoid the penetration through the abdomen, the dipole antenna was aligned horizontally. The distance between the feeding point of dipole antenna and model surface was 10 mm and the height of the feeding gap was set at the center of the fetal head to evaluate the worst-case scenario for the fetal head. The operating frequencies were 900 MHz and 2 GHz, because these are typical frequencies used in W-CDMA mobile phone systems. In this study, for the worst-case evaluation, the radiated powers were 0.25 W, which is the maximum output for a W-CDMA system. The cell size for the entire calculation region was  $2 \times 2 \times 2$  mm. The boundaries of the calculation region were formed using perfectly matched layer boundary conditions (eight layers). Figures 2(a), 2(b), and 2(c) illustrate the antenna positions in

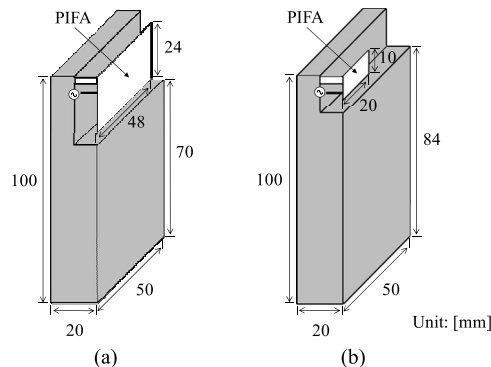


**Fig. 3** Dimensions of the wireless mobile terminal model used in the calculations. (a) For 900 MHz. (b) For 2 GHz.

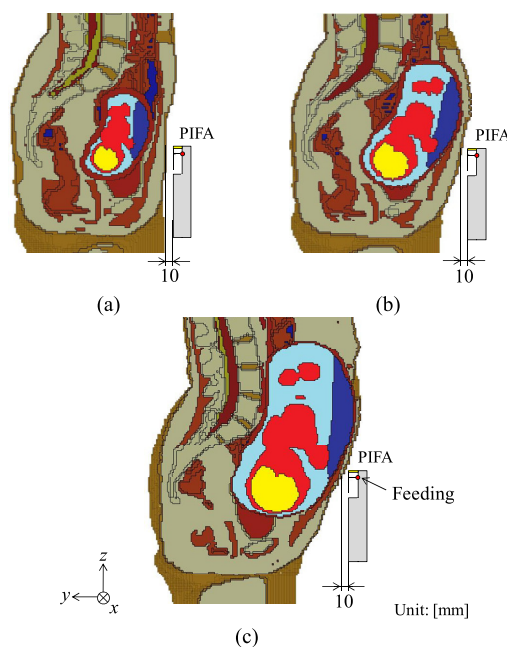


**Fig. 4** Positions of PIFAs in the sagittal plane including the feeding gap. Model at (a) 13th, (b) 18th, and (c) 26th gestational weeks.

the sagittal plane including the feeding gap for each model.

Figures 3(a) and 3(b) illustrate the wireless mobile terminal model with the PIFA. The operating frequencies were 900 MHz and 2 GHz. For both models, the size of the terminal was  $20 \times 50 \times 100$  mm. The calculation conditions, the height of the feeding gap and the distance between the radiated plate at the feeding and model surface were the same as those used in the analysis with the half-wavelength dipole antenna as like in Fig. 4. The radiated plate of the PIFA faced to the maternal abdomen.

### 3. SAR Calculation Results

#### 3.1 Half-Wavelength Dipole Antenna

Figure 5(a) shows the peak maternal and fetal 10-g-averaged SAR; the calculation method was the same as that used in

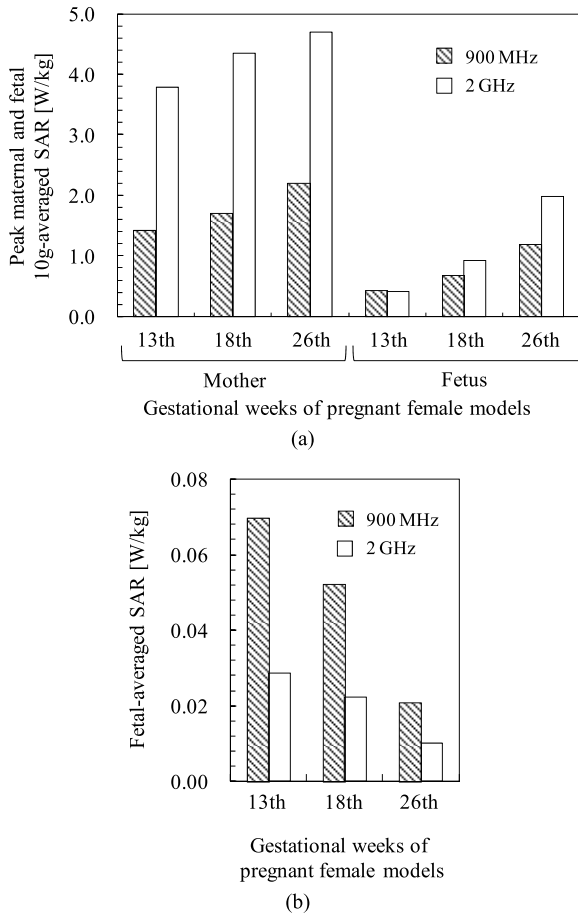


**Fig. 5** Computed values for SARs from the dipole antenna, (a) Peak maternal and fetal 10-g-averaged SAR, (b) Fetal-averaged SAR.

[30]. In all models, peaks in maternal SARs appeared on the skin nearest to the feeding point. The highest maternal SAR was approximately 4.70 W/kg in the 26th gestational week model at 2 GHz.

The peak in fetal SARs for both 900 MHz and 2 GHz in all three models also appeared on the fetal shoulder. The peak SAR in the 26th week model was the highest of the three models. The highest fetal value was approximately two-fifths of the highest maternal SAR value. Moreover, values of the 26th week model at 900 MHz and 2 GHz were approximately 2.8 times and 4.8 times higher than those of the 13th week model, respectively.

Figure 5(b) shows SARs averaged over whole fetal tissues (a body, a brain, and eyes) at 900 MHz and 2 GHz. In Fig. 5(b), the fetal-averaged SAR for the 13th week model was the highest of the three models. The fetal-averaged SARs for the three models at 900 MHz were 2.0–2.4 times higher than those at 2 GHz.

### 3.2 Planar Inverted-F Antenna

Figure 6(a) shows the peak maternal and fetal 10-g-averaged SARs from the PIFA. In all models, peak maternal SARs appeared on the skin nearest to the feeding point, just as

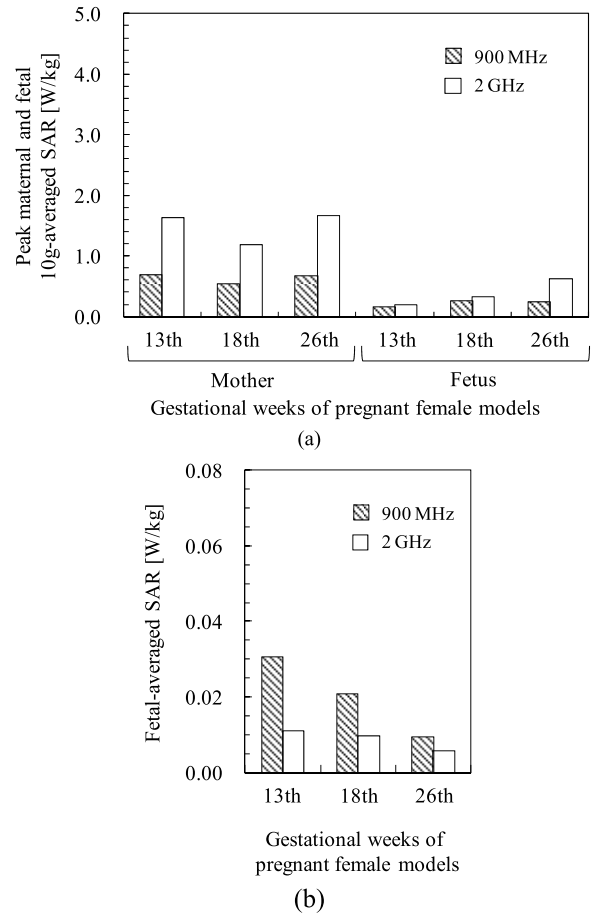


**Fig. 6** Computed values for SARs from the PIFA, (a) Peak maternal and fetal 10-g-averaged SAR, (b) Fetal-averaged SAR.

for the dipole antenna. The highest maternal SAR was approximately 1.66 W/kg in the 26th gestational week model at 2 GHz.

In all three models, the peak fetal SAR at 2 GHz was found to be around the fetal shoulder. In contrast, at 900 MHz, the peak SAR in the 13th and 26th gestational week models appeared at the fetal head, while the peak SAR in the 18th gestational week model appeared on the fetal shoulder (Fig. 8(a)). The value of the peak fetal 10-g-averaged SAR in the 26th gestational week model at 2 GHz was the highest among the three models. In contrast, at 900 MHz, the peak fetal 10-g-averaged SAR in the 26th gestational week model was lower than that in the 18th gestational week model; this differs tendency from the results obtained for the dipole antenna. The highest values in the 18th gestational week model at 900 MHz and the 26th gestational week model at 2 GHz were one-half and two-fifths of the highest maternal SAR value, respectively. Comparing results at both frequencies, values at 2 GHz were higher than those at 900 MHz.

Figure 6(b) shows the fetal-averaged SARs. Just as in Fig. 5(b) for the dipole antenna, the fetal-averaged SAR in the 13th gestational week model was higher than those in the other models. The fetal-averaged SARs for the PIFA at

900 MHz were 1.6–2.8 times higher than those at 2 GHz.

#### 4. Temperature Elevations

As previously mentioned, radio-frequency safety guidelines [1] for fetuses have not yet been established. To evaluate the safety of a fetus when a pregnant female is exposed to EM waves, it is necessary to determine temperature elevations in the fetus. A temperature elevation of 1°C–2°C that is due to the absorption of EM waves is known to be a root cause of adverse health effects such as heat exhaustion and heat stroke [1]. Furthermore, excessive maternal hyperthermia (such as thermal therapy for a tumor), including RF-induced hyperthermia, directly affects the growth of the embryo and the fetus [31]. According to [32], most animal data indicate that the implantation and development of the embryo and fetus are unlikely to be affected by exposures that increase maternal body temperature by less than 1°C. However, above this temperature increase, adverse effects such as growth retardation may occur. On the basis of this data, we set 1°C as the upper limit of the maximum temperature elevation allowed in the fetus.

Figure 7 presents the peak temperature elevations in the fetus. In this study, because we did not consider convection in the amniotic fluid, the temperature of the amniotic fluid continues to increase. Therefore, this temperature elevation is higher than would occur in the practical case; however, we can consider our calculation to serve as a simplified worst case. The peak temperature elevation increased with increasing gestational age; this trend corresponds to the trend in the peak fetal 10-g-averaged SAR (Fig. 5(a)). The highest peak temperature elevation was approximately 0.16°C for the 26th gestational week model at 2 GHz for dipole antenna. At both frequencies, the peak points of the fetal temperature elevations in the 13th and 18th gestational models appeared on the fetal head, and in the 26th gestational model appeared fetal shoulder.

The highest temperature elevation was in the 26th gestational week model at 2 GHz (0.09°C) for the PIFA. This value is approximately one-half of the highest temperature

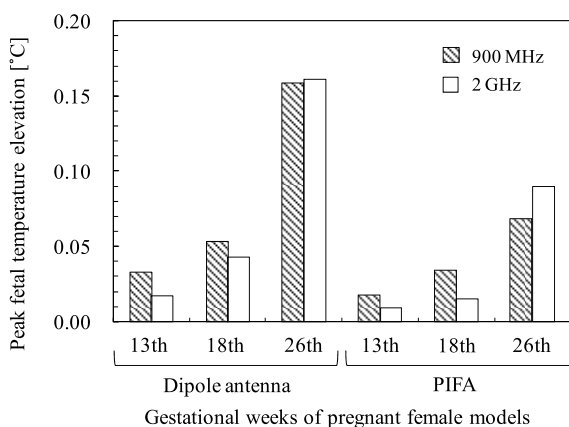


Fig. 7 Computed peak fetal temperature elevations for the dipole antenna and PIFA.

elevation for the dipole antenna. The tendency with processing gestational age is similar to the results for the dipole antenna. The peak points in the 13th and 18th gestational models appeared on the fetal head at both frequencies. On the other hands, the peak point in the 26th gestational model at 2 GHz appeared at the fetal shoulder, and that at 900 MHz appeared at the fetal head.

#### 5. Discussion

##### 5.1 Maternal SARs

Comparing the results for the dipole antenna and PIFA, the peak maternal 10-g-averaged SARs for the PIFA were 0.4–0.5 times lower than those for the dipole antenna. Maternal SARs from the dipole antenna and PIFA in each model are not in agreement because of difference in shapes of the maternal abdomen as gestation progresses. For dipole antenna, maternal SARs at 900 MHz (26th gestational week model) and at 2 GHz (13th, 18th, and 26th gestational week model) were above the RF guidelines (2 W/kg) for general public exposure. In this study, the output power was maintained constant at 0.25 W; however, the input impedance of the antenna changed in the vicinity of a human body. Therefore, the output power actually becomes lower than the input power. In contrast, all calculated maternal SARs from the PIFA were lower than the ICNIRP safety guideline.

##### 5.2 Fetal SARs

As gestational age increases, the peak fetal 10-g-averaged SARs for both the dipole antenna and the PIFA increased. This is because the distance between the peak point on the fetus and the EM source becomes shorter. However, this tendency did not occur in the SARs at 900 MHz for the PIFA. To explain this, note the angle of the fetus shown in Fig. 2(b); the fetal head in the 18th gestational week model was positioned deep in the maternal body and the fetal shoulder was positioned closer to the antenna in comparison with the other models. Therefore, the peak point of the fetal 10-g-averaged SAR in the 18th gestational week model at 900 MHz for the PIFA appeared at the fetal shoulder; in contrast, the peak points on the fetuses in 13th and 26th gestational weeks appeared at the head. Thus, the distance between the antenna and peak point at the fetal shoulder in the 18th gestational week model (32 mm) was shorter than the distance between the antenna and the peak point at the fetal head in the 26th gestational week model (36 mm). The peak fetal 10-g-averaged SAR in the 26th gestational week model for the dipole antenna was nearly equal to the RF guideline values for general public exposure because no consideration was given to the mismatch loss when the antenna was placed close to the human body, just as none was given to the maternal SARs.

For fetal whole-body averaged SARs, we found that differences between the fetal-averaged SARs for the dipole antenna and for PIFA have an approximately equal scaling

factor. As gestation progressed, the fetal-averaged SARs became lower from both EM sources. The main reason for this is that the fetal volume of the 13th week model is the smallest; therefore, the fetal-averaged SAR must be higher when the SAR is averaged over the whole fetal body. Comparing effects of frequencies, the fetal averaged SAR at 900 MHz was higher than that at 2 GHz in all cases in contrast to fetal 10-g-averaged SAR (Figs. 5(a) and 6(a)). This is because the wavelength at 900 MHz was longer than that at 2 GHz. Therefore, EM waves at 900 MHz more deeply penetrate the maternal body. Therefore, the area of high SAR at 900 MHz was larger than that at 2 GHz. The calculated fetal-averaged SARs in the 26th gestational week model were higher than the results in [7], because the SAR in the fetus strongly depends on the distance between the fetus and EM source. Also, [7] used the 26th gestational week model that was used in [9]; that model places the fetus more deeply in the maternal body. However, we confirmed that all averaged SARs in the fetuses were below the ICNIRP guideline limit (0.08 W/kg).

As described above, both fetal whole-body SAR and maximum 10-g-averaged SAR were lower for the PIFA than for the half-wavelength dipole antenna. Also, note that SAR values for the PIFA were lower than ICNIRP guideline limits.

### 5.3 Fetal Temperature Elevations

The peak point of the 10-g-averaged SARs in the 13th and 18th gestational week models appeared at the fetal shoulder, while the peak point of the temperature elevation in these models appeared at the fetal head. This is because the shoulders of fetuses in the 13th and 18th gestational week models are covered by the placenta, which provides cooling due to blood flow. However, the peak temperature elevation in the 26th gestational week model appeared at the fetal shoulder just as dose the peak point in the 10-g-averaged SAR of the 26th gestational week model, except for the peak in the 26th gestational week model for the PIFA at 900 MHz. As shown in Fig. 2, this is because the area of the fetal shoulder covered by the placenta in the 26th gestational week model was smaller than those in the 13th and 18th gestational week models. Therefore, the peak point in the 26th gestational week model appeared at the fetal shoulder, which is not covered with the placenta.

At 2 GHz, the peak temperature elevation in the fetus of the 26th gestational week model for the PIFA was higher than that of other models, because it reflects the trend of the peak fetal 10-g-averaged SAR (Fig. 6(a)), while the peak temperature elevation at 900 MHz did not follow this trend. The peak fetal 10-g-averaged SAR in the 18th gestational week model was higher than that in the 26th gestational week model; however, for the peak temperature, the value in the 18th gestational week model was lower than that in the 26th gestational week model. As shown in Fig. 8, which shows the surface SAR and temperature elevation distributions on the fetus of the 18th gestational week model, the

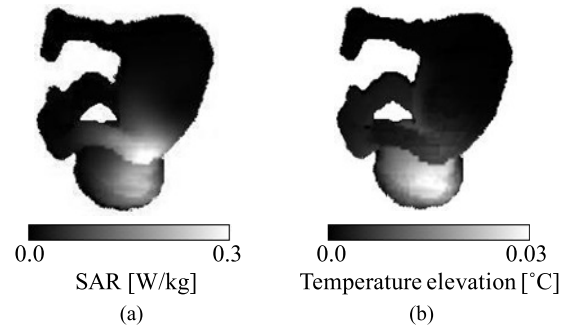


**Fig. 8** (a) Surface SAR and (b) surface temperature elevation distributions on the fetus at the 18th gestational week for the PIFA at 900 MHz.

peak SAR appeared on the fetal shoulder, but the peak temperature elevation did not appear on the fetal shoulder because of the cooling provided by the placenta. Therefore, the peak temperature elevation at 900 MHz did not correspond to the trend in the peak fetal 10-g-averaged SAR.

The maximum temperature elevation (0.16°C) was lower than our upper limit of 1°C. On comparing the fetal peak temperature elevation in the 26th gestational week model with the results in [8], our results are found to be lower than those in [8]. This is because the power radiated by the EM source, a professional VHF transceiver, in [8] was 20 times higher than ours.

## 6. Conclusions

In this study, we estimated SARs and temperature elevations in pregnant females and fetuses at three different gestation ages under exposure to EM waves from a wireless mobile terminal placed close to the abdomen of the pregnant female. The calculations were performed using the FDTD method. For these calculations, models of a Japanese pregnant female at 13th, 18th, and 26th week of gestation were used. As the radiator, we used a half-wavelength dipole antenna and PIFA with a constant radiated power of 0.25 W at both 900 MHz and 2 GHz. Local exposures in the fetus were sufficiently lower than those in the mother. When comparing the differences between the three gestational ages, the fetal-averaged SAR was higher in early pregnancy; however, the peak fetal 10-g-averaged SAR and the temperature elevation in the fetus were higher in late pregnancy. We also confirmed that exposures in the fetus using the dipole antenna were greater than those using the PIFA, because the gap feed of the PIFA was further away from the maternal body than the dipole antenna.

We found that the exposure of the fetus to EM waves was affected by the distance between the fetus and EM source. The fetal 10-g-averaged SAR in the 26th gestational week for the dipole antenna at 2 GHz was nearly equal to the recommended ICNIRP values for general public exposure. However, the peak temperature elevations were under the threshold (1°C), which could cause the birth of a child with developmental disabilities. In contrast, the PIFA did not create fetal SARs that approached the guidelines, and



temperature elevations from the PIFA were less than those created by the dipole antenna. We also note that, because of its advanced power control, the actual radiated power of a W-CDMA mobile phone was significantly lower than 0.25 W at both 900 MHz and 2 GHz. In future studies, we intend to investigate the effect of changing the position of the fetus and placenta. We will also evaluate the SAR in a fetus using an actual wireless mobile terminal because there may be differences between an actual mobile terminal and a PIFA.

## Acknowledgments

Part of this study was supported by the Strategic International Cooperative Program (Joint Research Type), of the Japan Science and Technology Agency.

## References

- [1] ICNIRP, "Guidelines for limiting exposure to time-varying electric, magnetic, and electromagnetic fields (0 Hz to 300 GHz)," *Health Phys.*, vol.74, no.4, pp.494–522, April 1998.
- [2] IEEE Standard for Safety Levels with Respect to Human Exposure to Radio Frequency Electromagnetic Fields, 3 kHz to 300 GHz, ANSI/IEEE Standard C95. 1-2005, Oct. 2005.
- [3] T. Nagaoka, S. Watanabe, K. Sakurai, E. Kunieda, S. Watanabe, M. Taki, and Y. Yamanaka, "Development of realistic high-resolution whole-body voxel models of Japanese adult males and females of average height and weight, and application of models to radio-frequency electromagnetic-field dosimetry," *Phys. Med. Biol.*, vol.49, pp.1–15, 2004.
- [4] P.J. Dimbylow, "FDTD calculations of the whole-body averaged SAR in an anatomically realistic voxel model of the human body from 1 MHz to 1 GHz," *Phys. Med. Biol.*, vol.42, pp.479–490, 1997.
- [5] A. Christ, W. Kainz, E.G. Hahn, K. Honegger, M. Zefferer, E. Neufeld, W. Rascher, R. Janka, W. Bautz, J. Chen, B. Kiefer, P. Schmitt, H. Hollenbach, J. Shen, M. Oberle, D. Szczerba, A. Kam, J.W. Guag, and N. Kuster, "The virtual family-development of surface-based anatomical models of two adults and two children for dosimetric simulation," *Phys. Med. Biol.*, vol.55, pp.N23–N38, 2010.
- [6] 2006 WHO Research Agenda for Radio Frequency Fields [http://www.who.int/entity/peh-emf/research/rf\\_research\\_agenda\\_2006.pdf](http://www.who.int/entity/peh-emf/research/rf_research_agenda_2006.pdf)
- [7] T. Togashi, T. Nagaoka, S. Kikuchi, K. Saito, S. Watanabe, M. Takahashi, and K. Ito, "FDTD calculations of specific absorption rate in fetus caused by electromagnetic waves from mobile radio terminal using pregnant woman model," *IEEE Trans. Microw. Theory Tech.*, vol.56, no.2, pp.554–559, Feb. 2008.
- [8] S. Akimoto, S. Kikuchi, T. Nagaoka, K. Saito, S. Watanabe, M. Takahashi, and K. Ito, "Evaluation of specific absorption rate for a fetus by portable radio terminal close to the abdomen of a pregnant woman," *IEEE Trans. Microw. Theory Tech.*, vol.58, no.12, pp.3859–3865, Dec. 2010.
- [9] T. Nagaoka, T. Togashi, K. Saito, M. Takahashi, K. Ito, and S. Watanabe, "An anatomically realistic whole-body pregnant-woman model and specific absorption rates for pregnant woman exposure to electromagnetic plane wave from 10 MHz to 2 GHz," *Phys. Med. Biol.*, vol.52, pp.6731–6745, Nov. 2007.
- [10] P.J. Dimbylow, "SAR in the mother and foetus for RF plane wave irradiation," *Phys. Med. Biol.*, vol.52, pp.3791–3802, July 2007.
- [11] P.J. Dimbylow, T. Nagaoka, and X.G. Xu, "A comparison of foetal SAR in three sets of pregnant female models," *Phys. Med. Biol.*, vol.54, pp.2755–2767, May 2009.
- [12] T. Nagaoka, K. Saito, M. Takahashi, K. Ito, and S. Watanabe, "Anatomically realistic reference models of pregnant woman for gestation ages of 13, 18, and 26 weeks," *Proc. 30th Annual Int. Conf. IEEE Eng. in Medicine and Biology Soc.*, pp.2817–2820, Aug. 2008.
- [13] H. Kawai, K. Ito, M. Takahashi, K. Saito, T. Ueda, M. Saito, H. Ito, H. Osada, Y. Koyanagi, and K. Ogawa, "Simple modeling of an abdomen of pregnant women and its application to SAR estimation," *IEICE Trans. Commun.*, vol.E89-B, no.12, pp.3393–3400, Dec. 2006.
- [14] J.L. Schepps and K.R. Foster, "The UHF and microwave dielectric properties of normal and tumour tissues: Variation in dielectric properties with tissue water content," *Phys. Med. Biol.*, vol.25, no.6, pp.1149–1159, Nov. 1980.
- [15] C. Gabriel, "Compilation of the dielectric properties of body tissues at RF microwave frequencies," Brooks Air Force Technical Report AL/OE-TR-1996-0037, 1996.
- [16] A. Peyman, C. Gabriel, H.R. Benedickter, and J. Fröhlich, "Dielectric properties of human placenta, umbilical cord and amniotic fluid," *Phys. Med. Biol.*, vol.56, p.N93, March 2011.
- [17] Basic anatomical and physiological data for use in radiological protection: reference values, ICRP Publication 89, 2002.
- [18] F.A. Duck, *Physical properties of tissue: A comprehensive reference book*, Academic Press, London, 1990.
- [19] H.H. Pennes, "Analysis of tissue and arterial blood temperature in resting forearm. 1948," *J. Appl. Physiol.*, vol.1, pp.5–34, July 1998.
- [20] J.W. Hand, Y. Li, E.L. Thomas, M.A. Rutherford, and J.V. Hajnal, "Prediction of specific absorption rate in mother and fetus associated with MRI examinations during pregnancy," *Magn. Reson. Med.*, vol.55, pp.883–893, April 2006.
- [21] D. Wu, S. Shamsi, J. Chen, and W. Kainz, "Evaluations of specific absorption rate and temperature increase within pregnant female models in magnetic resonance imaging birdcage coils," *IEEE Trans. Microw. Theory Tech.*, vol.54, no.12, pp.4472–4478, Dec. 2006.
- [22] V. Hombach, K. Meier, M. Burkhardt, E. Kuhn, and N. Kuster, "The dependence of EM energy absorption upon human head modeling at 900 MHz," *IEEE Trans. Microw. Theory Tech.*, vol.40, no.10, pp.1865–1873, Oct. 1996.
- [23] Q. Li and O.P. Gandhi, "Thermal implications of the new relaxed IEEE RF safety standard for head exposures to cellular telephones at 835 and 1900 MHz," *IEEE Trans. Microw. Theory Tech.*, vol.54, no.7, pp.3146–3154, July 2006.
- [24] A. Hirata, O. Fujiwara, and T. Shiozawa, "Correlation between peak spatial-average SAR and temperature increase due to antennas attached to human trunk biomedical engineering," *IEEE Trans.*, vol.53, no.8, pp.1658–1664, Aug. 2006.
- [25] A. Hirata and O. Fujiwara, "The correlation between mass-averaged SAR and temperature elevation in the human head model exposed to RF near-fields from 1 to 6 GHz," *Phys. Med. Biol.*, vol.54, pp.7227–7238, Nov. 2009.
- [26] P.M. Van Den Berg, A.T. De Hoop, A. Segal, and N. Praagman, "A computational model of electromagnetic heating of biological tissue with application to hyperthermic cancer therapy," *IEEE Trans. Biomed. Eng.*, vol.BME-30, pp.797–805, Dec. 1983.
- [27] P. Bernardi, M. Cavagnaro, S. Pisa, and E. Piuzzi, "Specific absorption rate and temperature elevation in a subject exposed in the far-field of radio-frequency sources operating in the 10–900-MHz range," *IEEE Trans. Biomed. Eng.*, vol.50, no.3, pp.295–304, March 2003.
- [28] K. Saito, Y. Hayashi, Y. Kanai, and J. Hori, "Fundamental heating characteristics of an RF hyperthermic system using a rectangular resonant cavity applicator for deep-seated tumors," *Jpn J Hyperthermic Oncol.*, vol.22, pp.1–11, 2006.
- [29] Y. Endo, K. Saito, S. Watanabe, M. Takahashi, and K. Ito, "Experimental evaluation of SAR around an implanted cardiac pacemaker caused by mobile radio terminal," *IEICE Trans. Commun.*, vol.E95-B, no.6, pp.2129–2132, June 2012.



- [30] IEEE Recommended Practice for Measurements and Computations of Radio Frequency Electromagnetic Field with Respect to Human Exposure to Such Field, 100 kHz–300 GHz, IEEE Standard C95.3-2002, 2003.
- [31] M.J. Edwards, R.D. Saunders, and K. Shiota, "Effects of heat on embryos and fetuses," *Int. J. Hypertherm.*, vol.19, no.3, pp.295–324, 2003.
- [32] "Environmental health criteria 137: Electromagnetic fields (300 Hz to 300 GHz)," WHO, Geneva, Switzerland, 1993.



**Akihiro Taten** was born in Chiba, Japan, in October 1988. He received the B.E. and M.E. degrees in electrical engineering from Chiba University, Chiba, Japan, in 2011 and 2013, respectively, and is currently working toward the Ph.D. degree at Chiba University. His main interests include the evaluation of the interaction between the EM field and human body.



**Shimpei Akimoto** was born in Tokyo, Japan, in April 1984. He received the B.E., M.E., and D.E. degrees in electrical engineering from Chiba University, Chiba, Japan, in 2007, 2009 and 2012, respectively. He is currently with Mitsubishi Electric Corporation, Kanagawa, Japan. His main interests include electrically small antennas and EM compatibility.



**Tomoaki Nagaoka** received the Ph.D. degree in medical science from Kitasato University, Kanagawa, Japan, in 2004. He is currently a Senior Researcher with the Electromagnetic Compatibility (EMC) Laboratory, Applied Electromagnetic Research Institute, National Institute of Information and Communications Technology, Tokyo, Japan. His main research interests include biomedical EM compatibility and medical image analysis. Dr. Nagaoka is a member of the IEEE Microwave Theory and Techniques Society (IEEE MTT-S), the IEEE Engineering in Medicine and Biology Society, and the Institute of Electronics, Information and Communication Engineers (IEICE), Japan. He was the recipient of several awards, including the 2004 Best Paper Award of Physics in Medicine and Biology, the 2007 Young Researcher Award of the IEICE, the 2008 Young Scientist Award of International Scientific Radio Union, the 2011 Outstanding Paper Award of the IEEE Africon and the 2011 Best paper award of the ISABELL' 11.



**Kazayuki Saito** was born in Nagano, Japan, in May 1973. He received the B.E., M.E., and D.E. degrees in electronic engineering from Chiba University, Chiba, Japan, in 1996, 1998 and 2001, respectively. He is currently an Associate Professor with the Research Center for Frontier Medical Engineering, Chiba University. His main interest is in the area of medical applications of microwaves including microwave hyperthermia. Dr. Saito is a member of the Institute of Electrical, Information and Communication Engineers (IEICE), Japan, the Institute of Image Information and Television Engineers of Japan (ITE), and the Japanese Society for Thermal Medicine. He was the recipient of the IEICE Antennas and Propagation Society (AP-S) Freshman Award, the Award for Young Scientist of the URSI General Assembly, the IEEE AP-S Japan Chapter Young Engineer Award, the Young Researchers' Award of the IEICE, and the International Symposium on Antennas and Propagation (ISAP) Paper Award in 1997, 1999, 2000, 2004, and 2005 respectively.



**Soichi Watanabe** received the B.E., M.E., and D.E. degrees in electrical engineering from Tokyo Metropolitan University, Tokyo, Japan, in 1991, 1993, and 1996, respectively. He is currently with the National Institute of Information and Communications Technology, Tokyo, Japan. His main research interest is biomedical EM compatibility. Dr. Watanabe is a member of the Institute of Electronics, Information and Communication Engineers (IEICE), Japan, the Institute of Electrical Engineers (IEE), Japan, and the Bioelectromagnetics Society. He was a member of the Standing Committee on Physics and Engineering of the International Commission on Non-Ionizing Radiation Protection (ICNIRP) since 2005 and now is a member of the Main Commission of the ICNIRP since 2012. He was the recipient of the 1996 Young Scientist Award of the International Scientific Radio Union, the 1997 Best Paper Award of the IEICE, and the 2004 Best Paper Award (The Roberts Prize) of Physics in Medicine and Biology.



**Masaharu Takahashi** was born in Chiba, Japan, in December 1965. He received the B.E. degree in electrical engineering from Tohoku University, Miyagi, Japan, in 1989, and the M.E. and D.E. degrees in electrical engineering from the Tokyo Institute of Technology, Tokyo, Japan, in 1991 and 1994, respectively. From 1994 to 1996, he was a Research Associate, and from 1996 to 2000, an Assistant Professor with the Musashi Institute of Technology, Tokyo, Japan. From 2000 to 2004, he was an Associate Professor with the Tokyo University of Agriculture and Technology, Tokyo, Japan. He is currently an Associate Professor with the Research Center for Frontier Medical Engineering, Chiba University, Chiba, Japan. His main interests are electrically small antennas, planar array antennas, and EM compatibility. Dr. Takahashi is a Senior Member of the Institute of Electronics, Information and Communication Engineers (IEICE), Japan. He was the recipient of the 1994 IEEE Antennas and Propagation Society (IEEE AP-S) Tokyo Chapter Young Engineer Award.



**Koichi Ito** received the B.S. and M.S. degrees from Chiba University, Chiba, Japan, in 1974 and 1976, respectively, and the D.E. degree from the Tokyo Institute of Technology, Tokyo, Japan, in 1985, all in electrical engineering. From 1976 to 1979, he was a Research Associate at the Tokyo Institute of Technology. From 1979 to 1989, he was a Research Associate at Chiba University. From 1989 to 1997, he was an Associate Professor at Chiba University, and is currently a Professor at the Department

of Medical System Engineering, Chiba University. From 2005 to 2009, he was Deputy Vice-President for Research, Chiba University. From 2008 to 2009, he was Vice-Dean of the Graduate School of Engineering, Chiba University. Since April 2009, he has been appointed as Director of Research Center for Frontier Medical Engineering, Chiba University. In 1989, 1994, and 1998, he visited the University of Rennes I, France, as an Invited Professor. He has been appointed as Adjunct Professor to the University of Indonesia since 2010. His main research interests include analysis and design of printed antennas and small antennas for mobile communications, research on evaluation of the interaction between electromagnetic fields and the human body by use of numerical and experimental phantoms, microwave antennas for medical applications such as cancer treatment, and antennas for body-centric wireless communications. Dr. Ito is a Fellow of the Institute of Electronics, Information and Communication Engineers (IEICE) of Japan, a member of the American Association for the Advancement of Science, the Bioelectromagnetics Society, the Institute of Image Information and Television Engineers of Japan (ITE) and the Japanese Society for Thermal Medicine. He served as Chair of the Technical Group on Radio and Optical Transmissions, ITE, from 1997 to 2001, Chair of the Technical Committee on Human Phantoms for Electromagnetics, IEICE, from 1998 to 2006, Chair of the Technical Committee on Antennas and Propagation, IEICE, from 2009 to 2011, Chair of the IEEE AP-S Japan Chapter from 2001 to 2002, Vice-Chair of the 2007 International Symposium on Antennas and Propagation (ISAP2007), General Chair of the 2008 IEEE International Workshop on Antenna Technology (iWAT2008), Co-Chair of ISAP2008, an AdCom member for the IEEE AP-S from 2007 to 2009, an Associate Editor for the IEEE Transactions on Antennas and Propagation from 2004 to 2010, a Distinguished Lecturer for the IEEE AP-S from 2007 to 2011 and General Chair of ISAP2012. He currently serves as Chair of the IEEE AP-S Committee on Man and Radiation (COMAR), and a Councilor to the Asian Society of Hyperthermic Oncology (ASHO). He has been elected as a delegate to the European Association on Antennas and Propagation (EurAAP) since 2012.